



HAL
open science

Accelerated molecular dynamics simulations of dislocation climb in nickel

T D Swinburne, Lauren Fey, Anne Marie Z. Tan, Thomas Swinburne, Danny
Perez, Dallas Trinkle

► **To cite this version:**

T D Swinburne, Lauren Fey, Anne Marie Z. Tan, Thomas Swinburne, Danny Perez, et al.. Accelerated molecular dynamics simulations of dislocation climb in nickel. *Physical Review Materials*, 2021, 5 (8), 10.1103/PhysRevMaterials.5.083603 . hal-03379938

HAL Id: hal-03379938






<https://hal.science/hal-03379938>

Submitted on 23 Nov 2023

HAL is a multi-disciplinary open access archive for the deposit and dissemination of scientific research documents, whether they are published or not. The documents may come from teaching and research institutions in France or abroad, or from public or private research centers.

L'archive ouverte pluridisciplinaire **HAL**, est destinée au dépôt et à la diffusion de documents scientifiques de niveau recherche, publiés ou non, émanant des établissements d'enseignement et de recherche français ou étrangers, des laboratoires publics ou privés.

Accelerated molecular dynamics simulations of dislocation climb in nickel

Lauren T. W. Fey ^{1,2,3} Anne Marie Z. Tan ^{1,4} Thomas D. Swinburne ^{5,3} Danny Perez ³ and Dallas R. Trinkle ^{1,*}¹*Department of Materials Science and Engineering, University of Illinois at Urbana-Champaign, Urbana, Illinois 61801, USA*²*Materials Department, University of California, Santa Barbara, Santa Barbara, California 93106, USA*³*Theoretical Division T-1, Los Alamos National Laboratory, Los Alamos, New Mexico 87545, USA*⁴*School of Mechanical and Aerospace Engineering, Nanyang Technological University, Singapore 639798, Singapore*⁵*Université Aix-Marseille, CNRS, CINaM UMR 7325, Campus de Luminy, 13288 Marseille, France*

(Received 14 October 2020; accepted 22 July 2021; published 9 August 2021)

The mechanical behavior of materials operating under high temperatures is strongly influenced by creep mechanisms such as dislocation climb, which is controlled by the diffusion of vacancies. However, atomistic simulations of these mechanisms have traditionally been impractical due to the long time scales required. To overcome these time scale challenges, we use Parallel Trajectory Splicing (ParSplice), an accelerated molecular dynamics method, to simulate dislocation climb in nickel. We focus on modeling the activity of a vacancy near a jog on an edge dislocation in order to observe vacancy pipe diffusion and vacancy absorption at the jog. From rigorously constructed trajectories encompassing more than 2000 vacancy absorption events over a simulation time of more than 4 μ s at 900 K, a comprehensive sampling of available atomistic mechanisms is collated and analyzed further with molecular statics calculations. We estimate average rates for pipe diffusion and vacancy absorption into the jog using data from the dynamic and static calculations, finding very good agreement. Our results strongly suggest that the dominant mechanism for vacancy absorption by jogs is via biased diffusion to the dislocation core followed by fast pipe diffusion to the jog.

DOI: [10.1103/PhysRevMaterials.5.083603](https://doi.org/10.1103/PhysRevMaterials.5.083603)

I. INTRODUCTION

At high temperatures, crystalline materials deform through a time-dependent process known as creep [1,2]. Understanding creep is critical for high-temperature applications, such as in the nickel superalloy turbine blades in jet engines [3–7]. These engines are more fuel efficient at higher temperatures, yet the operating temperatures are limited by the creep behavior of the component materials. Therefore, understanding creep mechanisms and rates is critical for advancing these applications. One mechanism of creep is dislocation climb, which involves the absorption of vacancies into dislocation cores, allowing dislocations to move out of their slip plane and glide around obstacles.

Simulations of dislocation climb are challenging due to the long time scales required. Dislocation climb requires the flux of vacancies through the bulk toward dislocations, which is a slow process compared to the nanosecond time scales for atomistic simulations. Dislocation jogs, which can be created thermally or by the intersection of dislocations, then absorb the vacancies in order to climb. These atomistic mechanisms are difficult to observe experimentally, so simulation techniques are necessary to advance our understanding. Most models of dislocation climb ignore the atomistic details of the dislocation climb mechanism but instead describe climb phenomenologically. Several groups have studied dislocation climb using dislocation dynamics methods [8–10]. Mordehai *et al.* was the first to couple dislocation dynamics with

vacancy diffusion [8], assuming that the rate-limiting step in dislocation climb is the bulk diffusion of vacancies to the dislocation lines. However, these models assume that vacancies can be absorbed anywhere along the dislocation line, ignoring the jog density and the rate of pipe diffusion, i.e., the potential acceleration of vacancy diffusion along the dislocation line. Pipe diffusion has been incorporated into some discrete dislocation dynamics models [11], but the interactions of vacancies with the jogs is not accounted for. Other modeling efforts for dislocation climb include phase field models [12,13]. These are also mesoscale models which do not explicitly include the atomistic mechanisms involved in dislocation climb, such as pipe diffusion and vacancy absorption at jogs. To parametrize and improve these models, the rates and mechanisms of the individual steps of dislocation climb must be understood.

Kabir *et al.* used atomistic methods to calculate the vacancy migration barriers near a dislocation and used the results to run kinetic Monte Carlo simulations [14]. Baker and Curtin coupled a discrete diffusion model to an accelerated molecular dynamics simulation to study the diffusion of vacancies to a dislocation and the nucleation of jogs [15]. However, this model did not include pipe diffusion due to limited length scales. Density functional theory has also been used to calculate the vacancy migration barriers for pipe diffusion [16], which were then used to parametrize a kinetic Monte Carlo model. These results show that pipe diffusion is orders of magnitude faster than bulk diffusion and can contribute to the overall creep rate when the dislocation density is high.

In this paper, we use ParSplice [17], an accelerated molecular dynamics technique, to study dislocation climb in nickel. ParSplice manages the production of many short,

*dtrinkle@illinois.edu

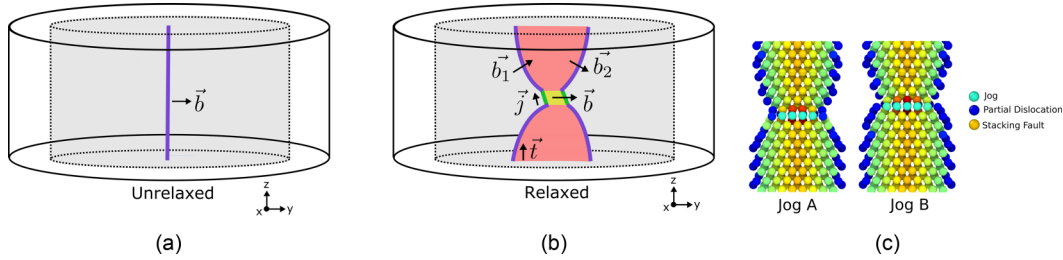


FIG. 1. (a) Schematic of the initial, unrelaxed dislocation system. A perfect edge dislocation with $\vec{b} = \frac{a}{2}[110]$ and line direction $N\vec{t} + \vec{j}$ (purple line) is introduced in a cylindrical simulation cell. The atoms in the gray region are then allowed to relax while all other atoms are held fixed. The simulation cell is aligned such that the periodic z direction is parallel to $N\vec{t} + \vec{j}$ and the y direction is parallel to $\vec{b} = \frac{a}{2}[110]$. (b) Schematic of the relaxed dislocation structure in the small system. The dislocation relaxes into an edge dislocation with a jog. The edge components dissociate into partial dislocations (purple) with $\vec{b}_1 = \frac{a}{6}[12\bar{1}]$ and $\vec{b}_2 = \frac{a}{6}[211]$. The stacking fault region between the partials is shown in red. The green dislocation lines represent the jog, which has a line direction of $\frac{a}{2}[1\bar{1}0]$. The extent of dissociation at the jog is much less than along the edge components, which has the effect of constricting the stacking fault region. (c) Comparison of the atomic configurations for the two different jog types. Atoms are colored by the centrosymmetry parameter with very low centrosymmetry atoms removed. The dark blue and green atoms surround the partial dislocations, and the yellow and orange atoms show the stacking fault regions. The two partial dislocations pinch together at the jog, which is shown by the red and turquoise atoms. Jog A is slightly more compact than Jog B, as can be seen by the turquoise atoms in the jog.

independently generated, molecular dynamics trajectories in parallel, which can then be rigorously “spliced” to form a single long trajectory between metastable states, thereby allowing for timewise parallelization and hence for long time simulations. The method is especially efficient to accelerate the production of escape trajectories from large superbases of energy minima. This is ideally suited to the problem we study here, namely, the thermally activated motion of a vacancy near an edge dislocation jog, a prototypical process in dislocation climb. From these simulations, we extract rates for vacancy pipe diffusion near and far from the jog site and further analyze found mechanisms for vacancy absorption and emission in the context of harmonic transition state theory via the use of static energy barrier calculations. It is important to emphasize that ParSplice generates long-time trajectories in a totally unbiased fashion. Indeed, every local basin of attraction on the potential energy surface is an allowed state and no restrictions are placed on possible transitions. The only factor that controls the accuracy of the method is the so-called *correlation time* τ_c used in the construction of the segments [17,18]; when states are defined as basins of attractions on the potential energy surface, τ_c is a characteristic vibrational timescale. It can be shown that the accuracy of the spliced trajectories increases exponentially with τ_c [18,19], so that the resulting trajectories can be made essentially MD-accurate if τ_c is chosen conservatively.

Our main result is that the vacancy flux to jog sites is dominated by biased vacancy diffusion to the dislocation line, followed by rapid pipe diffusion to the jog site. This is to be distinguished from vacancy diffusion to the jog site directly from the bulk. The implications of our findings for the multi-scale modeling of climb and therefore creep are discussed.

II. METHODS

In order to simulate the process of dislocation climb, an edge dislocation with a jog was created. All calculations are made using LAMMPS [20] with the Mishin EAM potential for nickel [21]. This potential was chosen for its known

ability to reproduce experimental values of the equilibrium lattice parameter, cohesive energy, elastic constants, intrinsic stacking fault energy, and bulk vacancy formation energy of face-centered cubic (FCC) nickel. An initially perfect edge dislocation with a total line vector of $N\vec{t} + \vec{j}$ was created in a cylinder, where \vec{t} is the line direction of the pure edge segment, \vec{j} is the line direction of the jog segment, and N is an integer Fig. 1(a). The dislocation has a Burgers vector of $\frac{a}{2}[110]$ and \vec{t} in the $\frac{a}{2}[1\bar{1}2]$ direction, so it lies in the $(\bar{1}11)$ slip plane. Since dislocation jogs can be formed by the intersection of dislocations, the jog has a line direction of $\frac{a}{2}[1\bar{1}0]$, a Burgers vector on a different slip plane in FCC. On relaxation, the initially straight dislocation line splits into pure edge segments and a jog segment, with the edge components dissociating into partial dislocations separated by a stacking fault [Fig. 1(b)]. This partial decomposition lowers the line energy of the dislocation, but it leaves a stacking fault region between the two partial dislocations. At the jog, the two edge dislocations are closer together due to the higher stacking fault energy on the (001) plane. In the stacking fault region, the stacking of atomic planes resembles hexagonal close packing instead of the equilibrium FCC packing of nickel. For this reason, it is useful to use the centrosymmetry parameter as a visualization tool. The centrosymmetry parameter measures the inversion symmetry around each atom, giving zero for perfect FCC crystals and higher values near defects such as dislocations or vacancies; removing atoms with low centrosymmetry allows us to isolate the defective regions. Interestingly, depending on the plane in which the jog exists, two different jog configurations can be formed. These will be referred to as Jog A and B [Fig. 1(c)]. The two jog configurations arise due to the two distinct (001) planes on which the jog, with a line direction of $\frac{a}{2}[1\bar{1}0]$, can intersect the dislocation line. Both jog configurations have the same partial splitting distance of 19.3 Å far from the jog, but Jog A is slightly more compact than Jog B, as can be seen by counting the number of atoms shown in the jogged region. When a jog absorbs a vacancy, the jog is displaced by one half a dislocation threading vector. Two vacancy absorption events are required to return to the

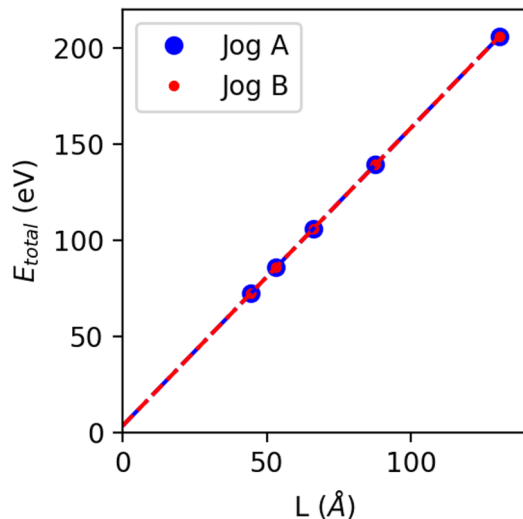


FIG. 2. The total energy of the jogged edge dislocation as a function of the total dislocation length. Extrapolating the linear fit to a dislocation of length zero gives the energy of the jog only. The energy for both Jog A and Jog B is 3.52 eV.

original configuration and displace the jog a full threading vector.

The total energy of the system includes contributions from the cohesive bulk energy, the dislocation line energy, and the jog energy. The jog energy was estimated for each jog configuration by calculating the total energy of the system for different N , which controls the jog-jog distance. Extrapolating to an isolated jog with a distance of 0 gives the energy of the jog only without the edge dislocation segments (Fig. 2). The energy for both Jog A and Jog B is 3.52 eV. Therefore, which configuration a jog forms is determined by geometric considerations only.

Two different system sizes were created: A large system with approximately 120,000 atoms and a smaller system with approximately 16,000 atoms. The smaller system was used for the accelerated molecular dynamics simulations to reach longer timescales, while the larger system was used to verify the results through molecular statics simulations. During all simulations, periodic boundary conditions are applied along the dislocation line, while fixed boundary conditions are used perpendicular to the dislocation line. The fixed boundary conditions are implemented by fixing an outer ring of atoms at positions prescribed by the anisotropic elastic solution for a perfect edge dislocation [22]. In the large system, this corresponds to a 60 Å radius cylinder being simulated, while the smaller system has a radius of 30 Å. The lengths of the dislocations lines were also varied by adjusting N , the number of pure edge segment threading vectors. For the large system, N is 15, and for the small system, N is 8. To ensure that the small system size is still representative of a dislocation in bulk, the energy barrier for pipe diffusion was calculated for both system sizes using the nudged elastic band method (NEB) [23,24]. The initial and final states of the NEB were taken directly from the ParSplice simulations. The average of the forward and reverse barriers is 0.86 eV for the large system and 0.87 eV for the small system, suggesting that

pipe diffusion is not significantly impacted by the change in system size. Additionally, the jog splitting distance, defined as the distance between the two partial dislocations at the jog, is similar for the two system sizes. Using Ovito's dislocation analysis tool [25], the two atomic sites where the dislocation lies closest to the jog were identified, and the distance between these two sites is defined as the jog splitting distance. For Jog A, this distance is 11.7 and 11.6 Å for the small and large systems, respectively. For Jog B, the respective values are 14.0 and 14.1 Å. Therefore, we feel confident that performing the accelerated MD in the small system will still yield results that are representative of behavior in the bulk.

We used ParSplice [17], an accelerated molecular dynamics method, to simulate a vacancy near the jogged dislocation and calculate rates of vacancy pipe diffusion and absorption rates. The simulations were run at 900 K using a Langevin thermostat with a timestep of 2 fs. Each ParSplice simulation used 200 replicas with four cores assigned to each replica. The correlation time used was 2 ps. In each simulation, a vacancy was added to the system at an atomic site near or inside the partial dislocations. Each vacancy site was chosen manually using the centrosymmetry parameter to identify the dislocation line. Figure 1(c) shows these partial dislocation sites in dark blue. Each state identified by ParSplice was automatically analyzed to determine the position of the vacancy. This is done by identifying a cluster of atoms that are all missing a nearest neighbor in approximately the same location. An atom is considered to be missing a nearest neighbor if the sum of its vectors to nearest neighbors has a magnitude greater than 0.75 Å. The position of the vacancy is estimated as the mean position of these missing neighbors. If the vacancy position moves less than 0.1 Å between consecutive ParSplice events, those states are considered the same for the purposes of vacancy diffusion. This automatic vacancy identification method allows for many simulations to be statistically analyzed together to calculate vacancy diffusion rates. In addition to the 900 K simulations, selected simulations were also run at 800 and 1000 K to evaluate entropic effects.

To support the ParSplice simulation results, we also perform molecular statics calculations on the larger jogged dislocation system. Vacancy-dislocation interaction energies near the dislocation, which measure the energy change of a vacancy due to the nearby dislocation, were calculated. The interaction energy can be predicted using elasticity theory for vacancy positions far from the dislocation; however, near the dislocation, elasticity theory breaks down and atomic simulations are required to accurately determine these interaction energies [26]. The interaction energies were calculated for a variety of lattice sites by measuring the total energy of the system with vacancy at that site. The interaction energy is given by

$$E_{D+V}^{\text{int}} = E_{D+V} - E_D + E_0 - E_V^F, \quad (1)$$

where E_{D+V}^{int} is the interaction energy, E_{D+V} is the total energy of the dislocation-vacancy system, E_D is the energy of system with no vacancy, E_0 is the cohesive energy, and E_V^F is the bulk vacancy formation energy.

Additionally, the energy barriers for vacancy movement within the dislocation and jog were calculated with the NEB

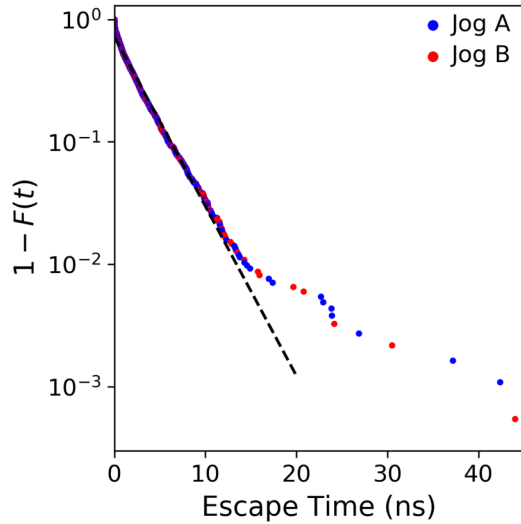


FIG. 3. Distribution of vacancy hopping times. $F(t)$ is the cumulative probability distribution. The majority of the data show a linear relation, showing that the main vacancy diffusion process follows a Poisson distribution. The slope of the plotted black line is $-\tau^{-1}$, where τ is 3.14 ns.

method [23,24]. Starting and ending configurations were chosen for specific vacancy events: pipe diffusion along the dislocation line, vacancy absorption into the jog, vacancy movement out of the slip plane, etc. An initial path is created by linearly interpolating between the starting and ending configurations.

III. RESULTS AND DISCUSSION

Using the relaxed dislocation system, we performed ParSplice simulations and observed the vacancy diffusing along the partial dislocations and being absorbed into the jogs. By using this accelerated MD technique, we are able to achieve total simulation times of over 2.7 and 1.6 μs for vacancies diffusing and absorbing into Jog A and Jog B, respectively. In each simulation, the vacancy diffuses randomly along the partial dislocation cores until it reaches the jog and is absorbed. The vacancy spends the vast majority of the simulation time on the compressive side of the dislocation, and any hops across the slip plane are quickly followed by hops back to the compressive side. After the jog absorbs the vacancy, it will occasionally emit vacancies, which are always immediately reabsorbed. In total, 1843 vacancy hops along the partials and 18 initial vacancy absorptions were observed during the combined simulation time. Including vacancy reabsorption, there were a total of 510 vacancy absorptions.

We are first interested in how the vacancy diffuses within the partial dislocations. The vacancy escape time is defined as the amount of time between vacancy hops within the partial dislocations. The escape times for every simulation are calculated, not including hops into or out of the jog, and are plotted in Fig. 3. Occasionally, the observed vacancy diffusion took place in the bulk or outside of the slip plane instead of within the dislocation because the vacancy jumped out of the dislocation line. In these cases, the vacancy always returns to the dislocation line as opposed to diffusing away into the bulk

since vacancy has a lower energy within the dislocation. These outliers were removed in order to study only the pipe diffusion mechanism. The overall mean escape time was 2.34 ns. For Jog A, the mean escape time was 2.31 ns \pm 0.10 ns, and the mean escape time for Jog B was 2.39 ns \pm 0.19 ns. Therefore, there is no discernible difference between pipe diffusion behavior in dislocations with Jog A versus Jog B.

If we assume that vacancy diffusion within the partial cores is a constant rate Poisson process where the energy barriers for pipe diffusion are constant and not significantly impacted by the presence of the jog, then the escape times should follow an exponential distribution,

$$F(t) = 1 - e^{-t/\tau}, \quad (2)$$

where t is the escape time, $F(t)$ is the cumulative probability distribution, and τ is the average time between events. The vast majority of the 1843 vacancy escape times recorded fall below 15 ns. In this region, the plot is linear with a slope corresponding to $\tau = 3.14$ ns, supporting the assumption that vacancy diffusion is a Poisson process. The long tail of escape times greater than 15 ns can be attributed to more rare events such as vacancy hopping in and out of the partial dislocation cores. These events will have a different average escape time and therefore do not fall on the linear fit. Additionally, there is a cluster of escape times less than 0.025 ns that also do not fall on the linear fit, which is attributed to the increased hopping rate for vacancies near the jog. Therefore, the linear portion with $\tau = 3.14$ ns corresponds to pipe diffusion along the dislocation line independent of the presence of the jog.

To better quantify the impact of the jog on vacancy diffusion, we study how the distance from the jog affects the direction of vacancy flow. At each point along the dislocation line, the number of vacancies passing by in the positive and negative z directions is calculated. Figure 4 shows the fraction of these vacancies that are observed traveling in the positive z direction. For random vacancy diffusion, this fraction should be near 0.5, which can be seen for positions far from the jog. However, within about 10 \AA of the jog, this value deviates from 0.5 as the jog biases the direction of diffusion. Because the jog attracts vacancies, vacancies are more likely to flow toward the jog. While vacancy pipe diffusion is random and vacancy hops in both directions occur on either side of the jog, the jog creates a diffusion flux for vacancies near the jog.

To estimate the free-energy difference between the jog and the displaced jog + vacancy state, we ran simulations starting with a jog only to observe vacancy emission, reaching a total of 38.5 μs of simulation time (Table I). The free-energy difference can be estimated by comparing the amount of time spent in each state:

$$\Delta G = k_B T \ln \left(\frac{t_{\text{jog}}}{t_{\text{jog+vac}}} \right), \quad (3)$$

where t_{jog} is the simulation time spent in the jog only state and $t_{\text{jog+vac}}$ is the time spent in the displaced jog + vacancy state. To investigate possible entropy effects, the same simulations with a jog only were repeated at 800 and 1000 K. Table I shows that Jog B undergoes a larger free-energy change on emitting a vacancy at all three temperatures studied. The results do not show a strong temperature dependence for

TABLE I. Vacancy emission from the jog. At all temperatures, Jog A emitting a vacancy has a lower free-energy difference than Jog B emitting a vacancy. This causes Jog A to have a significantly higher vacancy emission rate than Jog B.

Process	Jog A \rightarrow Jog B + Vacancy			Jog B \rightarrow Jog A + Vacancy		
	800	900	1000	800	900	1000
Temperature (K)	800	900	1000	800	900	1000
Total simulation time (μ s)	11.5	16.1	5.76	18.3	22.4	11.1
Number of vacancies emitted	81	402	162	27	162	257
Vacancy emission rate (μ s $^{-1}$)	7.04	25.0	28.1	1.48	7.23	23.2
Free-energy difference (eV)	0.814 ± 0.007	0.818 ± 0.004	0.828 ± 0.004	0.918 ± 0.011	0.884 ± 0.023	0.910 ± 0.007

either jog configuration, suggesting that entropic effects are minimal.

To complement the ParSplice results, we also performed molecular statics calculations. First, vacancy-dislocation interaction energies were calculated for a variety of atomic sites in a straight edge dislocation and jogged dislocation. The interaction energy describes the difference in energy for a vacancy at a specific site relative to a vacancy in the bulk, so the vacancies will be attracted to areas with more negative interaction energies. For both dislocation types, the interaction energies outside of the dislocation correspond to the stress state around the dislocation, with tensile regions having positive interaction energies and compressive regions having negative interaction energies. Inside the dislocation cores, the interaction energies are much larger. In a straight edge dislocation, the interaction energy of a site within the core is -0.34 eV, while in the jogged dislocation, the interaction energy at a site within the core but far from the jog is -0.37 eV. This suggests that the jog has a small effect on vacancies at sites far from the jog. As was observed in the ParSplice simulations, the vacancy is attracted to the dislocation cores due to their negative interaction energies, and the vacancies

were unlikely to hop out of the dislocation core due to the associated energy penalty. The highest magnitude interaction energies are found at sites directly adjacent to the jog. For Jog A, there are two equivalent sites on either side of the jog, each with an interaction energy of -0.58 eV. Between these two sites, there are four sites where, if the vacancy is placed there, it is absorbed and the jog displaces. These four sites correspond to the four atoms behind the turquoise atoms in Fig. 1(c). For Jog B, there are also two sites on either side of the jog with an interaction energy of -0.66 eV. However, due to symmetry, there are only three sites where the vacancy is absorbed, and these atoms are also found behind the row of turquoise atoms in Fig. 1(c). These strongly negative interaction energies suggest that the vacancy will be attracted to the jog. Overall, the calculated interaction energies show that vacancies are naturally attracted to the partial dislocations and jog.

The energy barriers for vacancy hops in and around the dislocation were calculated for a variety of positions in the system. Four distinct types of hops are identified and their energy barriers are shown in Fig. 5. The energy barrier for vacancy migration in the bulk is 1.29 eV, and all four of the vacancy events shown have much lower barriers so will therefore occur much more quickly than bulk diffusion. The first hop shows a vacancy diffusing along the length of the partial dislocation, referred to as pipe diffusion. The energy barrier for pipe diffusion is nearly symmetric with a barrier of approximately 0.86 eV. We find that the jog has little effect on the barrier for pipe diffusion, as the barrier in a jog-free edge dislocation was also calculated to be 0.86 eV. For a hop across the slip plane, the energy increases since the vacancy moves from a compressive region to a tensile region, which is consistent with the interaction energy calculations performed previously. The final two barriers show a vacancy being absorbed from either the bulk or the stacking fault. Both show that the total energy is lowered when the vacancy is in dislocation cores. Together, these results support the ParSplice observation of vacancy attraction to the partial dislocation core followed by pipe diffusion.

These calculated barriers can be compared to the ParSplice results by transition state theory, which states that the rate is related to the energy barrier by

$$\Gamma = \nu_0 e^{-\frac{\Delta E}{kT}}, \quad (4)$$

where Γ is the rate, ν_0 is a frequency prefactor, and ΔE is the energy barrier. Assuming a barrier of 0.86 eV for pipe diffusion and an average time between events of 3.14 ns, transition state theory predicts ν_0 to be $2.1 \times 10^{13} \text{ s}^{-1}$ at 900 K. This

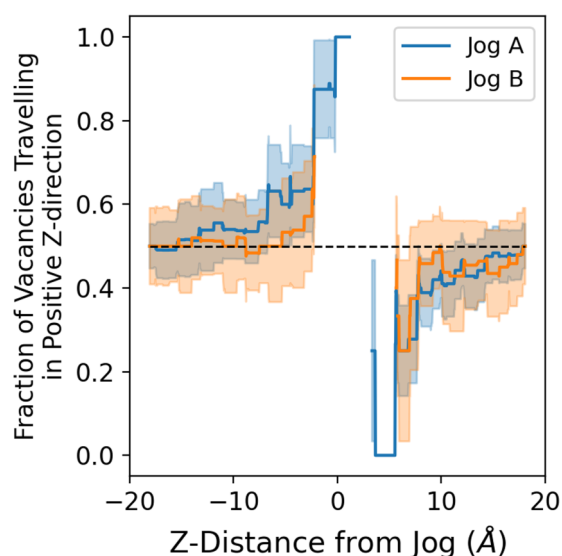


FIG. 4. The fraction of vacancies hopping in the positive z direction as a function of distance along the dislocation line. The shaded region shows the standard error. Far from the jog, this fraction is about 0.5, so there is no directional preference for vacancy hopping. Closer to the jog, the vacancies are more likely to hop toward the jog than away, showing that the jog biases the vacancy diffusion direction.

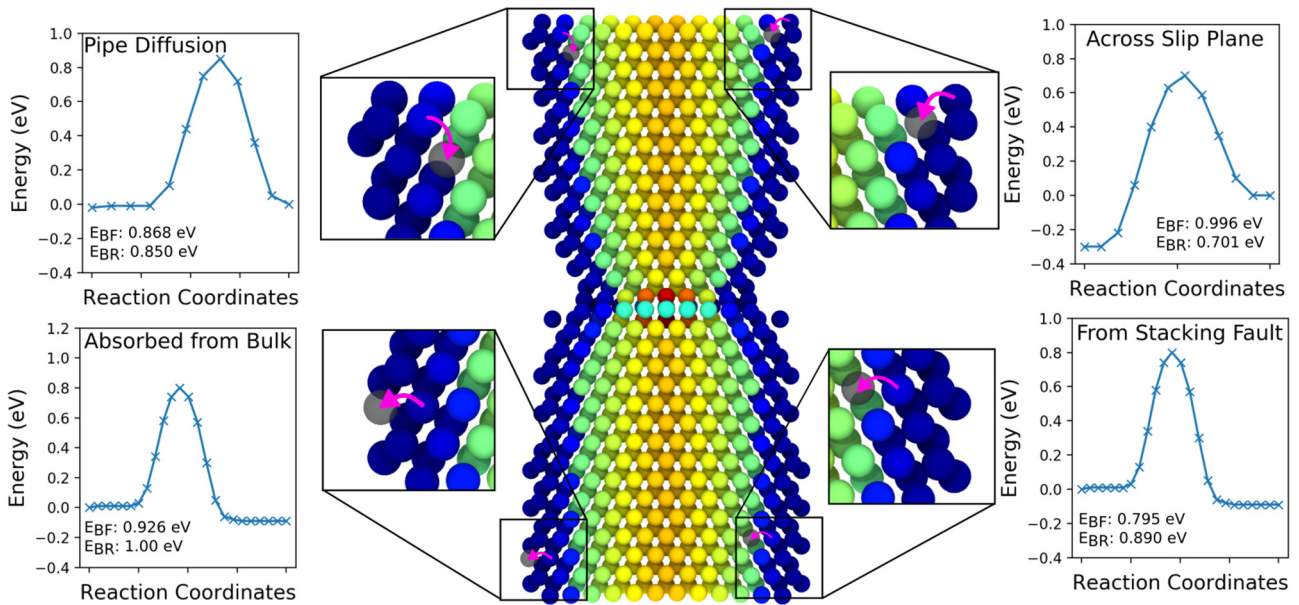


FIG. 5. NEB-calculated energy barriers for vacancy hops in and around the partial dislocations. The arrow shows the direction of motion for the atom that replaces the vacancy. Compared to the bulk vacancy diffusion barrier of 1.29 eV, all of these vacancy hopping events have much lower barriers. The total energy is lowered when the vacancy is absorbed into the partial dislocation from either the stacking fault or the bulk, which is consistent with the interaction energy calculation. The vacancy also prefers to be on the compressive side of the slip plane, as shown by the barrier for movement across the slip plane. The barrier for pipe diffusion is approximately 0.86 eV, which suggests that pipe diffusion along the partial dislocations will be much faster than bulk diffusion.

value of ν_0 is in good agreement with the typical estimation of $\nu_0 = 10^{13} \text{ s}^{-1}$, showing that the assumption of a Poisson process is valid and consistent with the NEB-computed energy barrier of 0.86 eV.

The NEB method was also used to calculate the energy barrier for a vacancy being emitted from the jog. The energy profile associated with emitting a vacancy from each jog configuration is slightly different, as shown in Fig. 6. Since the

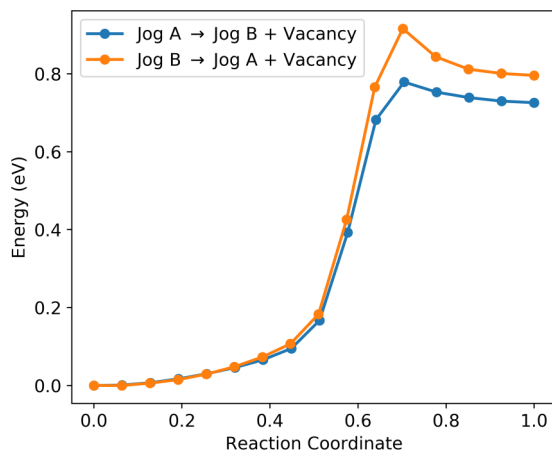


FIG. 6. NEB-calculated energy profile of a vacancy being emitted from each jog configuration. The barriers for vacancy emission are 0.916 eV for Jog B and 0.779 eV for Jog A. Conversely, the barriers for vacancy absorption are relatively low at 0.120 eV for a vacancy absorbed into Jog A and 0.053 eV for a vacancy absorbed into Jog B.

two jogs have the same energy, both curves begin at 0 eV, but the ending energies are different due to the difference in vacancy interaction energies for sites near the jog as discussed previously. The barriers for vacancy emission are comparable to pipe diffusion, 0.779 eV for a vacancy emitted from Jog A and 0.916 eV for a vacancy emitted from Jog B. Based on these calculations, Jog A would be expected to emit vacancies more often than Jog B, which is consistent with the ParSplice emission rates shown in Table I.

The barriers for the reverse process, vacancy absorption, are relatively small. The absorption barrier for a vacancy being absorbed by Jog A is 0.120 and 0.053 eV for a vacancy being absorbed by Jog B. We can compare the average absorption time predicted by transition state theory to that calculated with ParSplice. Assuming ν_0 is 10^{13} s^{-1} , the average absorption time is 0.470 ps for Jog A and 0.198 ps for Jog B at 900 K. This is consistent with ParSplice calculations as the vast majority of vacancies emitted are reabsorbed within one ParSplice segment (1 ps). Since the absorption time is on the scale of picoseconds while the vacancy hopping time is on the nanosecond scale, the rate-limiting step for dislocation climb will be vacancy diffusion to the jog, not absorption into the jog.

The NEB-calculated energy difference at 0 K can be compared to the free-energy difference calculated by ParSplice (Table I). The 0 K energy differences are 0.726 eV for Jog A and 0.796 eV for Jog B. At 900 K the ParSplice-calculated free-energy difference is only 0.092 eV higher for Jog A, and 0.088 eV higher for Jog B. These small differences can be attributed to entropic effects. The agreement between these two methods of calculation again supports the ParSplice results.

IV. CONCLUSION

Accelerated molecular dynamics and molecular statics were used to study a vacancy near a jogged edge dislocation in nickel in order to observe dislocation climb. Two different jog configurations with identical energies are formed due to the geometry of the lattice, and absorption of a vacancy causes the dislocation to climb and change jog configurations. We used ParSplice, an accelerated molecular dynamics method, to simulate a vacancy diffusing along the dislocation line to the jog. At 900 K, the mean time for pipe diffusion was 3.14 ns, which is consistent with transition state theory estimates using the NEB-calculated barriers of 0.86 eV for pipe diffusion. By comparison, the TST-estimated bulk diffusion time is 1.67 μ s. Once the vacancy has diffused to the jog, it is absorbed very quickly, on the picosecond scale, due to the low-energy barriers for vacancy absorption. Therefore, assuming vacancies are present in the dislocation line, pipe diffusion will be the rate-limiting step. The jog can also emit vacancies, but these were always reabsorbed in our simulations due to the high attraction between the jog and the vacancy. The free-energy differences between the jog state and the vacancy plus displaced jog state were calculated at 800, 900, and 1000 K. The free-energy difference for Jog B emitting a vacancy is greater than Jog A, and the free-energy differences do not show a strong temperature dependence. The energy differences calculated with ParSplice are consistent with those calculated via molecular statics and strongly suggest that vacancy absorption to jogs is

dominated by biased diffusion to the dislocation line followed by fast pipe diffusion to the jog. These results can be used to parametrize future mesoscale models to better understand dislocation climb in complex systems.

ACKNOWLEDGMENTS

This work was partially supported by the Science Undergraduate Laboratory Internships program from the Department of Energy Office of Science. This work was also supported by the Illinois Scholars Undergraduate Research Program, and the Department of Energy National Nuclear Security Administration Stewardship Science Graduate Fellowship, which is provided under cooperative agreement number DE-NA0003960. Work at Los Alamos National Laboratory was supported by the Laboratory Directed Research and Development program of Los Alamos National Laboratory under Project No. 20150557ER. Los Alamos National Laboratory is operated by Triad National Security, LLC, for the National Nuclear Security Administration of U.S. Department of Energy (Contract No. 89233218CNA000001).

This research is part of the Blue Waters sustained-petascale computing project, which is supported by the National Science Foundation (awards OCI-0725070 and ACI-1238993) and the state of Illinois. Blue Waters is a joint effort of the University of Illinois at Urbana-Champaign and its National Center for Supercomputing Applications.

-
- [1] M. A. Meyers, *Dynamic Behavior of Materials* (John Wiley & Sons, New York, 1994).
 - [2] P. Haasen, *Physical Metallurgy*, Third ed. (Cambridge University Press, Cambridge, 1996), translated by J. Mordike.
 - [3] P. Caron and T. Khan, Improvement of creep strength in a nickel-base single-crystal superalloy by heat treatment, *Mater. Sci. Eng.* **61**, 173 (1983).
 - [4] T. M. Pollock and A. S. Argon, Creep resistance of CMSX-3 nickel base superalloy single crystals, *Acta Metall. Mater.* **40**, 1 (1992).
 - [5] T. Murakumo, T. Kobayashi, Y. Koizumi, and H. Harada, Creep behaviour of Ni-base single-crystal superalloys with various γ' volume fraction, *Acta Mater.* **52**, 3737 (2004).
 - [6] C. M. F. Rae and R. C. Reed, Primary creep in single crystal superalloys: Origins, mechanisms and effects, *Acta Mater.* **55**, 1067 (2007).
 - [7] T. M. Smith, Y. Rao, Y. Wang, M. Ghazisaeidi, and M. J. Mills, Diffusion processes during creep at intermediate temperatures in a Ni-based superalloy, *Acta Mater.* **141**, 261 (2017).
 - [8] D. Mordehai, E. Clouet, M. Fivel, and M. Verdier, Introducing dislocation climb by bulk diffusion in discrete dislocation dynamics, *Philos. Mag.* **88**, 899 (2008).
 - [9] S. Gao, M. Fivel, A. Ma, and A. Hartmaier, 3D discrete dislocation dynamics study of creep behavior in Ni-base single crystal superalloys by a combined dislocation climb and vacancy diffusion model, *J. Mech. Phys. Solids* **102**, 209 (2017).
 - [10] K. Danas and V. S. Deshpande, Plane-strain discrete dislocation plasticity with climb-assisted glide motion of dislocations, *Model. Simul. Mater. Sci. Eng.* **21**, 045008 (2013).
 - [11] Y. Gao, Z. Zhuang, Z. L. Liu, X. C. You, X. C. Zhao, and Z. H. Zhang, Investigations of pipe-diffusion-based dislocation climb by discrete dislocation dynamics, *Int. J. Plast.* **27**, 1055 (2011).
 - [12] J. H. Ke, A. Boyne, Y. Wang, and C. R. Kao, Phase field microelasticity model of dislocation climb: Methodology and applications, *Acta Mater.* **79**, 396 (2014).
 - [13] P. A. Geslin, B. Appolaire, and A. Finel, A phase field model for dislocation climb, *Appl. Phys. Lett.* **104**, 011903 (2014).
 - [14] M. Kabir, T. T. Lau, D. Rodney, S. Yip, and K. J. Van Vliet, Predicting Dislocation Climb and Creep from Explicit Atomistic Details, *Phys. Rev. Lett.* **105**, 095501 (2010).
 - [15] K. L. Baker and W. A. Curtin, Multiscale diffusion method for simulations of long-time defect evolution with application to dislocation climb, *J. Mech. Phys. Solids* **92**, 297 (2016).
 - [16] L. J. Wirth, A. A. Farajian, and C. Woodward, Density functional study of self-diffusion along an isolated screw dislocation in fcc Ni, *Phys. Rev. Materials* **3**, 033605 (2019).
 - [17] D. Perez, E. D. Cubuk, A. Waterland, E. Kaxiras, and A. F. Voter, Long-time dynamics through parallel trajectory splicing, *J. Chem. Theory Comput.* **12**, 18 (2016).
 - [18] C. Le Bris, T. Lelievre, M. Luskin, and D. Perez, A mathematical formalization of the parallel replica dynamics, *Monte Carlo Methods Appl.* **18**, 119 (2012).
 - [19] D. Perez, B. P. Uberuaga, and A. F. Voter, The parallel replica dynamics method—Coming of age, *Comput. Mater. Sci.* **100**, 90 (2015).
 - [20] Steve Plimpton, Fast parallel algorithms for short-range molecular dynamics, *J. Comput. Phys.* **117**, 1 (1995)

- [21] Y. Mishin, D. Farkas, M. J. Mehl, and D. A. Papaconstantopoulos, Interatomic potentials for monoatomic metals from experimental data and ab initio calculations, *Phys. Rev. B* **59**, 3393 (1999).
- [22] D. Bacon, D. Barnett, and R. Scattergood, Anisotropic continuum theory of lattice defects, *Prog. Mater. Sci.* **23**, 51 (1980).
- [23] G. Henkelman and H. Jónsson, Improved tangent estimate in the nudged elastic band method for finding minimum energy paths and saddle points, *J. Chem. Phys.* **113**, 9978 (2000).
- [24] G. Henkelman, B. P. Uberuaga, and H. Jónsson, Climbing image nudged elastic band method for finding saddle points and minimum energy paths, *J. Chem. Phys.* **113**, 9901 (2000).
- [25] A. Stukowski, Visualization and analysis of atomistic simulation data with OVITO—the Open Visualization Tool, *Modell. Simul. Mater. Sci.* **18**, 015012 (2010).
- [26] E. Clouet, The vacancy-edge dislocation interaction in fcc metals: A comparison between atomic simulations and elasticity theory, *Acta Mater.* **54**, 3543 (2006).